

LEWIS RESEARCH CENTER  
IN-32-CR

326309

P47



# A Planar Near-Field Scanning Technique for Bistatic Radar Cross Section Measurements

S. Tuhela-Reuning and E.K. Walton

The Ohio State University

## ElectroScience Laboratory

Department of Electrical Engineering  
Columbus, Ohio 43212

Technical Report 723105-1  
Grant No. NAG3-1125  
December 1990

National Aeronautics and Space Administration  
Lewis Research Center  
21000 Brookpark Road  
Cleveland, Ohio 44135

(NASA-CR-187794) A PLANAR NEAR-FIELD  
SCANNING TECHNIQUE FOR BISTATIC RADAR CROSS  
SECTION MEASUREMENTS (Ohio State Univ.)

47 D

CSCL 20N

N91-16194

Unclass

63/32 0326309

## NOTICES

When Government drawings, specifications, or other data are used for any purpose other than in connection with a definitely related Government procurement operation, the United States Government thereby incurs no responsibility nor any obligation whatsoever, and the fact that the Government may have formulated, furnished, or in any way supplied the said drawings, specifications, or other data, is not to be regarded by implication or otherwise as in any manner licensing the holder or any other person or corporation, or conveying any rights or permission to manufacture, use, or sell any patented invention that may in any way be related thereto.

<b>REPORT DOCUMENTATION PAGE</b>	<b>1. REPORT NO.</b>	<b>2.</b>	<b>3. Recipient's Accession No.</b>
<b>4. Title and Subtitle</b> A Planar Near-Field Scanning Technique for Bistatic Radar Cross Section Measurements		<b>5. Report Date</b> December 1990	
<b>7. Author(s)</b> S. Tuhela-Reuning and E.K. Walton		<b>6.</b>	
<b>9. Performing Organization Name and Address</b> The Ohio State University ElectroScience Laboratory 1320 Kinnear Road Columbus, OH 43212		<b>8. Performing Org. Rept. No.</b> 723105-1	
<b>12. Sponsoring Organization Name and Address</b> National Aeronautics and Space Administration Lewis Research Center 21000 Brookpark Rd., Cleveland OH 44135		<b>10. Project/Task/Work Unit No.</b>	
		<b>11. Contract(C) or Grant(G) No.</b> (C) (G) NAG3-1125	
		<b>13. Report Type/Period Covered</b> Technical Report	
<b>15. Supplementary Notes</b>		<b>14.</b>	
<b>16. Abstract (Limit: 200 words)</b>			
<p>This is a progress report on the development of a bistatic RCS measurement range. A technique using one parabolic reflector and a planar scanning probe antenna is analyzed. The field pattern in the test zone is computed using a spatial array of signal sources. It achieved an illumination pattern with 1 dB amplitude and 15° phase ripple over the target zone. The required scan plane size is found to be proportional to the size of the desired test target. Scan plane probe sample spacing can be increased beyond the Nyquist <math>\lambda/2</math> limit permitting constant probe sample spacing over a range of frequencies.</p>			
<b>17. Document Analysis a. Descriptors</b>			
NEAR-FIELD		PLANAR SCANNING	
BISTATIC RCS			
ARRAY ANTENNA			
<b>b. Identifiers/Open-Ended Terms</b>			
<b>c. COSATI Field/Group</b>			
<b>18. Availability Statement</b> A. Approved for public release; Distribution is unlimited.		<b>19. Security Class (This Report)</b> Unclassified	<b>21. No. of Pages</b> 46
		<b>20. Security Class (This Page)</b> Unclassified	<b>22. Price</b>



# Contents

List of Figures	v
List of Tables	vi
<b>1 Introduction</b>	<b>1</b>
<b>2 Scanner Design Issues</b>	<b>6</b>
2.1 Introduction . . . . .	6
2.2 Scan Plane Size . . . . .	6
2.3 Probe Measurement Spacing . . . . .	7
2.4 Position Accuracy . . . . .	9
2.5 Probe Characteristics . . . . .	10
2.6 Scanner to Test Target Separation Distance . . . . .	10
2.6.1 Evanescent waves . . . . .	10
2.6.2 Multiple Interactions . . . . .	11
2.7 Conclusions . . . . .	12
<b>3 Planar Scanner Simulation</b>	<b>13</b>
3.1 Introduction . . . . .	13
3.2 Theory . . . . .	13
3.3 Tests Implemented . . . . .	14
3.4 Results . . . . .	17
3.4.1 Taper Effects . . . . .	17
3.4.2 Sample Spacing . . . . .	20
3.4.3 Aperture Size . . . . .	26
3.4.4 Down Range Variation . . . . .	26
3.4.5 Outside Design Frequency Band . . . . .	26

11

<b>4</b>	<b>Conclusions</b>	<b>32</b>
<b>5</b>	<b>Future Work</b>	<b>33</b>
5.1	Scanner Construction . . . . .	33
5.2	RCS Calibration Technique . . . . .	33
<b>APPENDIX</b>		
<b>A</b>	<b>C Program Listing</b>	<b>37</b>

# List of Figures

1	Bistatic Scattering Arrangement . . . . .	2
2	Scan Plane Reference Coordinates . . . . .	5
3	Simulation Equation Development . . . . .	15
4	Visualization of Taper Function . . . . .	16
5	Bistatic RCS Measurement Facility with Planar Scanner . .	18
6	Normalized E-Field Amplitude and Phase, Comparison of Different Amounts of Amplitude Taper . . . . .	19
7	Normalized E-Field Amplitude and Phase, Comparison of Different Amounts of Phase Taper . . . . .	21
8	Normalized E-Field Amplitude and Phase, Comparison of Different Sample Spacings at 1 GHz . . . . .	23
9	Normalized E-Field Amplitude and Phase, Comparison of Different Sample Spacings at 10 GHz . . . . .	24
10	Normalized E-Field Amplitude and Phase, Comparison of Different Sample Spacings at 18 GHz . . . . .	25
11	Normalized E-Field Amplitude and Phase, 1 GHz Down Range Response Comparison . . . . .	27
12	Normalized E-Field Amplitude and Phase, 18 GHz Down Range Response Comparison . . . . .	28
13	Normalized E-Field Amplitude and Phase, 0.5 GHz Response: Below Design Frequency Band . . . . .	30
14	Normalized E-Field Amplitude and Phase, 35 GHz Response: Above Design Frequency Band . . . . .	31

# List of Tables

1	Position Accuracy Requirements . . . . .	9
2	Scan Plane Array Antenna Amplitude Taper Response, 90°	20
3	Scan Plane Array Antenna Phase Taper Response, 12% . .	20
4	Scan Plane Array Antenna Sample Spacing Variation Response	22
5	Scan Plane Array Antenna Down Range Performance . . .	29
6	Scan Plane Array Antenna Performance Outside Design Band	29

# Chapter 1

## Introduction

This progress report supports the development of a bistatic radar cross section (bistatic RCS) measurement range by PMTC Milicon-P986 under NASA Lewis Research Center contract #NAG3-1125. The bistatic scattering measurement scenario under consideration is shown in Figure 1. As shown in this figure, a compact range consisting of a parabolic reflector and a spherical wave feed will be used to generate a plane wave that illuminates the target. The incident plane wave signal is bistatically scattered from the target under test. The bistatic RCS measurement system must then determine the far-field scattered signal in the bistatic direction.

Many methods exist to estimate the far-field scattered signal without the distances necessary to measure the actual far-fields. One frequently used method is the reception of a plane wave by a compact range reflector. Other methods include using a one-dimensional vertical parabolic panel, such as a bent rod, scanned in a radial manner around the target. This measurement method requires a one dimensional near-field to far-field transformation algorithm. Another alternative is to scan the scattered fields along a

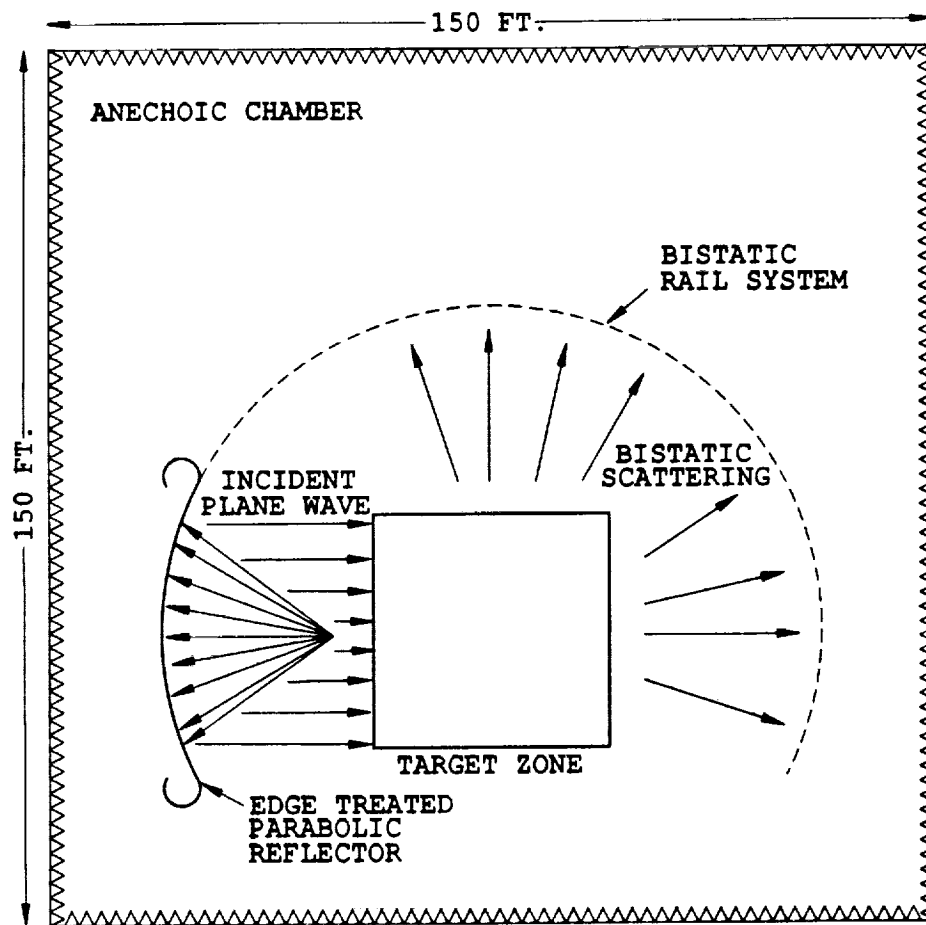


Figure 1: Bistatic Scattering Arrangement

spherical, cylindrical or planar surface with a probe antenna and transform the measurements to the far-field. Each of these surface scans require a two dimensional transformation algorithm, but planar scanning does not require curved sampling paths and it uses a well known near-field to far-field transformation algorithm, the heart of which is a two-dimensional Fourier transform [2]. A fourth alternative is synthesis of a plane wave by an antenna array, recreates the aperture distribution of a compact range reflector. In considering each of these alternatives it is necessary to determine the effects of finite scan area and sample spacing.

Note the similarity of these last two alternatives to the classical planar near-field technique for antenna pattern measurement. Upon illumination of the scatter by the plane wave, the scatterer becomes a radiator. It is behaving like an antenna. This means that much of the planar near-field technology developed for antenna pattern measurements is applicable to this research. For the measurement of antenna patterns, knowledge of the gain of the antenna is required such that the pattern function can be normalized to the total radiated energy. Thus if 85% of the energy is received by the scan surface, the gain can be well estimated. For the measurement of RCS however, only the plane wave incident at the given bistatic (or monostatic) angle is required. This is accomplished by any planar aperture large enough to reduce edge effect errors. Therefore, a RCS measurement system need not receive 80 to 85% of the radiated energy from the target. A RCS measurement system is calibrated by the theoretical RCS predictions of known test targets.

In this progress report, planar near-field scanning will be considered.

The scan plane with reference coordinates is shown in Figure 2. Reciprocity indicates that if an antenna array can simulate a compact range antenna pattern, then the antenna array should also receive signals similarly to a compact range reflector.

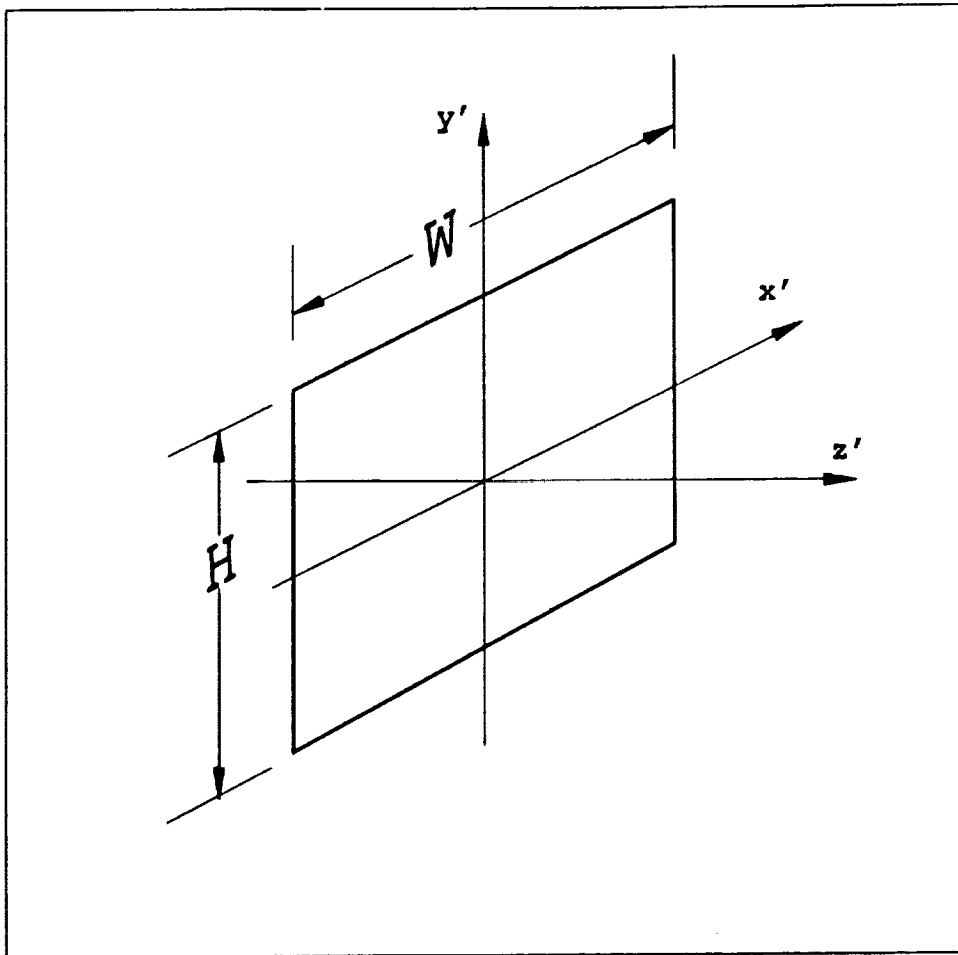


Figure 2: Scan Plane Reference Coordinates

# Chapter 2

## Scanner Design Issues

### 2.1 Introduction

Scan plane size (array size), probe measurement spacing (array element spacing), position accuracy, probe characteristics (array element characteristics), and the distance from the scanner (or array) to the test target all effect the scanner system and an antenna array system similarly during the design stage.

### 2.2 Scan Plane Size

In classical near-field antenna pattern measurements, near-field to far-field transformations, such as Kern's Plane Wave Spectrum matrix approach [10], direct determination of the source distribution at the target, or the Lorentz reciprocity formulation developed by Paris, Leach and Joy [7] can be used to estimate the far-field scattered signal from the measured scan plane data. To quantize the magnitude of the error involved in these transformations over a finite scan plane, Yaghjian [8] suggests performing the transformation

algorithm on the area outside the scan plane. Since the fields outside the scan plane are not known, the error is estimated as the “a priori” knowledge of the energy not received by the scan plane. This criterion is frequently used to require retaining 80 to 85% of the radiated energy within the scan surface and limit test targets to ones that radiate directly.

In this work, the array size and spatial windowing designs will be chosen to mimic the behavior of a compact range reflector. The array size requirement is thus the same as for a compact range reflector: the plane wave region must cover the test target entirely. For identical target (quiet) zones, the necessary scan plane size is expected to be comparable with a compact reflector surface (including rolled edges).

The size of the plane wave region in the target zone is proportional to the size of the scan plane. A useful plane wave region is often characterized by a 1 dB amplitude ripple and 10 degree phase ripple. In the literature, Johnson et.al. [1] quotes Woonton as having a minimum scan-plane to target-zone size ratio of 2.0, Chapman 2.3, and Georgia Tech 1.9. Joy and Rowland [3] used a minimum scan-plane to target-zone ratio of 1.7 for a highly directive parabolic dish target. Thus, as a general rule of thumb, the scan-plane must be twice the size of the largest target to be measured.

## **2.3 Probe Measurement Spacing**

The planar scanner receives the incident scattered fields at discrete sample points. To satisfy the Nyquist sampling criterion, samples should be taken at intervals which are equal to or less than one half the wavelength. Cown

and Ryan [9] however, note that “thinned” near-field data sets can be used to find accurate RCS values over reduced angular sectors. The grating lobes that occur due to the increased sample spacing are outside the region of interest and are simply ignored. If the incident planar-wavefront angles are restricted to a small range of angles about the normal of the scan surface, the sample spacing can be increased beyond the half-wavelength criteria.

The maximum acceptable sampling can be found from geometrical considerations. Since the signals of interest are confined to angles near the normal to the scan plane, the sample spacing should be such that neighboring array elements are  $180^\circ$  out of phase when the incident angle approaches the boundary of the region of interest. This is the first null of the array pattern. The sample spacing is given by:

$$\Delta S_{max} = \frac{\lambda}{2 \cos(\frac{\pi}{2} + \theta)}$$

where  $\theta$  is the incidence angle. The resulting grating lobes are located at incidence angles  $\phi$ :

$$\phi = \frac{\pi}{2} \pm \arccos\left(\frac{n\lambda}{\Delta S}\right); \quad n = 1, 2, 3, \dots$$

For the PMTC specifications, the target zone width is 20 feet at a distance of 59 feet from the scan plane aperture. Thus, the maximum angle of interest is roughly 10 degrees from the scan plane normal and the maximum acceptable sample spacing is  $2.8\lambda$ .

Table 1: Position Accuracy Requirements

f [GHz]	$\lambda$ [m]	$\lambda/10$ [mm]	$\lambda/360$ [mm]
0.5	0.6000	60.00	0.1667
1.0	0.3000	30.00	0.0833
18.0	0.0167	1.666	0.0463
35.0	0.0086	0.857	0.0238
phase error	360°	36°	1°

## 2.4 Position Accuracy

Near field position must be known to within a small fraction of a wavelength to obtain accurate field measurements. For system frequencies of 1 to 18 GHz, the minimum wavelength is 1.667 cm. For a maximum 1° error in the out of scan-plane direction, the  $z'$  coordinate must have 0.046 mm accuracy. For a maximum 10% $\lambda$  error and the additional requirement of 1.667 mm accuracy across the diagonals, the allowable error in  $x'$  and  $y'$  directions can be found to be  $1.6/\sqrt{2} = 1.17$  mm. This assumes independence of  $(x',y')$  and  $z'$  errors. These results are summarized in Table 1. Note that the highest frequency of interest is the limiting factor.

Note that phase measurement errors and cable bending errors can be modeled as  $z'$  coordinate errors. Bearden and Dugenske [5] report that Georgia Tech has a 1° accuracy over their scan plane. Yaghjian [8] notes that position error may be reduced by scanning along both vertical and horizontal lines and appropriately averaging the two data sets. This however, doubles data set measurement times. An important concern is re-

positioning accuracy, necessary for background subtraction algorithms (if needed) and system reliability. All errors must be contained such that the total effective error is within the tolerances stated above.

## 2.5 Probe Characteristics

Johnson et.al. [1 pp.1671] suggest the following probe characteristics: (1) Small aperture for point measurement and broad beam width. (2) Polarization should be accurate and stable. (3) Probes the size of  $\lambda/2$  dipoles or smaller are needed for accurate measurements but probes with more directivity than  $\lambda/2$  dipoles produce large measurement errors.

To reduce the time required for each data set scan, different scanning antennas can be used. Cown and Ryan in [9] suggest the use of arrays of modulated scattering elements or scanning antenna arrays to accomplish one or two of the dimensions of the scan plane. The data measurement times for these antennas are shown to be reduced by a factor of approximately 100 in comparison to scanning with a single probe antenna. [9 pp.580 Fig.8]

## 2.6 Scanner to Test Target Separation Distance

### 2.6.1 Evanescent waves

An evanescent wave's constant phase plane is not parallel to its direction of arrival. Thus their propagation constant can be greater than  $k_o$ , the free-space propagation constant along a given direction [6]. Incident angles ignored in the sample spacing computations may also correspond to

evanescent mode propagation constants. Due to these abnormalities, the evanescent wave effects should be minimized. One solution is to place the antenna array far enough away from the scatterer such that the evanescent waves are attenuated by the distance. Joy and Paris [3] formulated the minimum attenuation of the evanescent waves at a distance,  $N\lambda$ .

$$\alpha_{min} = 8.7N\lambda(k_m^2 - k_o^2)^{\frac{1}{2}} \quad [dB]$$

where

$$k_o^2 < k_m^2 \leq k_x^2 + k_y^2$$

$$k_x^2 = k_o^2 \sin^2 \theta \cos^2 \phi$$

$$k_y^2 = k_o^2 \sin^2 \theta \sin^2 \phi$$

Note that  $\sin^2 \theta$  is greater than 1.

## 2.6.2 Multiple Interactions

Multiple interactions are all the possible reflection paths from the target to the scan plane via walls, support structures, etcetera. Multiple interactions can be reduced by increasing the scan surface to target distance, using efficient absorber, decreasing probe size and averaging the results of scans fractions of a wavelength apart in the  $z'$  direction. To experimentally estimate the effect of multiple bounce interactions, Yaghjian [8] suggests varying the spacing between the scan plane and target as a function of the wavelength. Amplitude variations of period one half wavelength will be caused primarily by double bounce reflections.

## 2.7 Conclusions

We have mentioned some of the important parameters to consider in the design of a near field scanner. Joy [4] makes an exhaustive list of parameters, some of the more notable being: (1) Record the position, amplitude and phase of the probe to implement error compensation algorithms. (2) Smooth motion of the probe antenna will minimize vibration. (3) Motion can induce Doppler effects on the frequencies. (4) Allow for measurement of both polarizations. (5) Test facility temperature should be held constant with minimal gradients. (6) Teflon has a phase anomaly at room temperature.

# Chapter 3

## Planar Scanner Simulation

### 3.1 Introduction

We modeled the planar near-field scanner as an antenna array in the transmitting mode, generating a plane wave region in the target zone. By reciprocity and the duality of a scanning probe and an antenna array, the planar near-field scanner receive pattern is similar to the transmission pattern of the antenna array. Thus, use of the transmitting viewpoint to design the planar scanner is justified.

### 3.2 Theory

The simulation is accomplished by a point by point application of Maxwell's wave equation solution in free space for spherical wave propagation. Each field point in the quiet zone is the resultant sum of contributions from each source element antenna in the scan plane. The equation used to model the antenna array system is described in Figure 3. Normalization of the  $E_n$  sources in the scan plane by  $N$ , the number of array elements, gives a

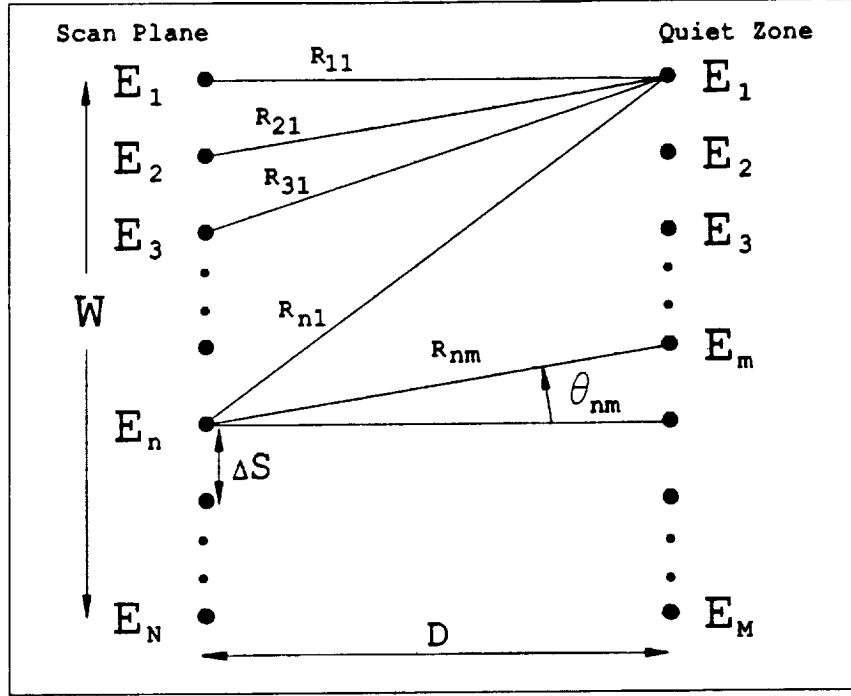
constant output power independent of the numbers of array elements.

The amplitude and phase taper functions were chosen to simulate the edge treatment effects of a compact range reflector with rolled edges. In a rolled edge compact range, the reflector geometry transitions from a parabolic surface, which produces a constant phase and amplitude reflected signal, to a rolled edge, which produces an increasing phase delay and a decreasing amplitude. In the planar scanner taper function a similar transition from constant phase and amplitude to phase and amplitude tapering occurs.

This taper function,  $T(n)$ , is used to spatially filter the measured data to suppress measurement sidelobes. The taper function is illustrated in Figure 4. The amplitude taper implemented is a cosine squared rolloff which characteristically has low side lobes, and the phase taper is a cosine function drop off with a frequency independent phase delay characteristic. A given taper function is denoted as the percentage of the scan plane width,  $x\%$  of  $W$  and the maximum phase delay (MPD) in degrees, for example 14%, 90°.

### 3.3 Tests Implemented

The figures to be discussed are one-dimensional cuts through what is, in practice, a two-dimensional pattern. These patterns are the E-field amplitude and phase that result in the quiet zone from the excitation of the array antenna in the scan plane. The normalized E-field amplitude is given in units of dB/m which means  $20 \log_{10}(V/m)$  where  $V/m$  is the measured



$$E_m = \sum_{n=1}^N \frac{E_n}{N} T(n) P(\theta_{nm}) \frac{e^{jkR_{nm}}}{R_{nm}}$$

where

- $T(n)$  = Taper function
- $P(\theta_{nm})$  = Scan plane element pattern function
- $\theta_{nm}$  = angle of line joining  $n^{th}$  and  $m^{th}$  elements
- $k$  = free space propagation constant
- $R_{nm}$  = distance between  $n^{th}$  and  $m^{th}$  elements
- $N$  = Number of elements in scan plane
- $D$  = distance between scan plane and quiet zone
- $\Delta S$  = Scan plane element spacing

Figure 3: Simulation Equation Development

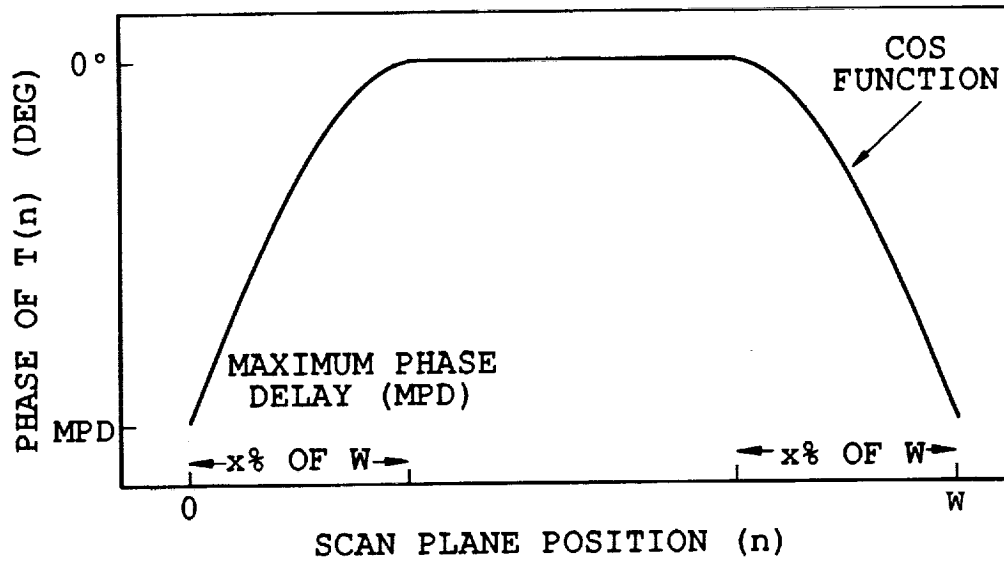
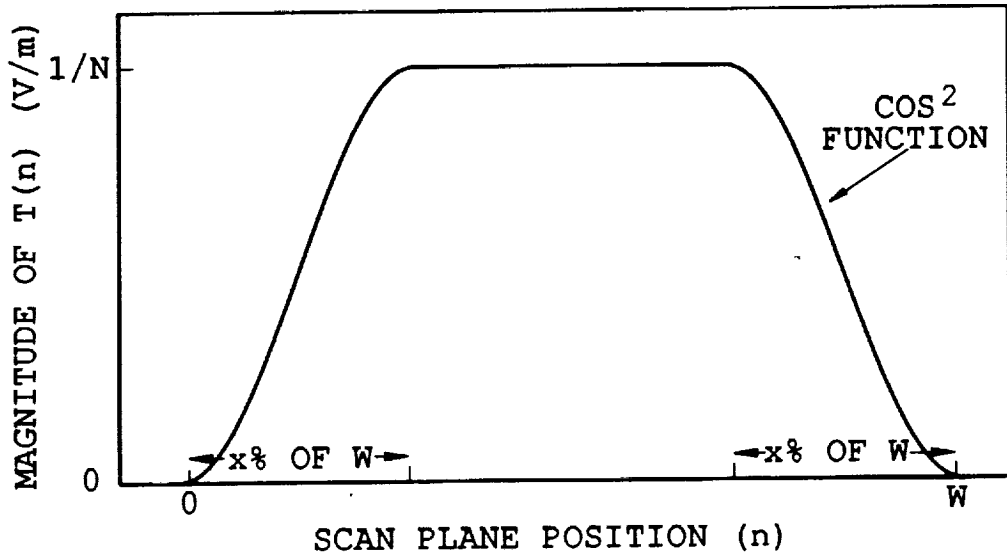


Figure 4: Visualization of Taper Function

E-field amplitude. The E-field phase is referenced to the scan plane and is given in degrees. The constant parameters of the simulations presented are: (1) The scan plane array element pattern function is set to 1 for all  $\theta_{nm}$ , simulating an isotropic radiator. (2) The scan plane width,  $W$  is nominally 8.5 m or approximately 40 ft. The physical dimensions used were closely matched to the design specifications of the PMTC Milicon-P986 Bistatic RCS measurement range. See Figure 5.

We investigated the effects of (1) amplitude and phase taper variations, (2) increasing the element spacing,  $\Delta S$ , beyond  $\lambda/2$ , (3) changing the distance between the test zone and scan plane, and (4) the response of the model to frequencies outside the design frequency band. In each case, the aperture size attained,  $W_{qz}$ , is discussed. Comparison is made with the characteristics of the compact range reflector with rolled edges at the Ohio State University as reported by Burnside et.al. [11].

## 3.4 Results

### 3.4.1 Taper Effects

The first parameter investigated was the amount of amplitude taper which gave the largest quiet zone for a 1 dB,  $10^\circ$  approximation to a plane wave. The frequency was chosen to be 1 GHz as a worst case where the ripple would be greatest. The phase taper was held constant at  $90^\circ$  while the amplitude taper was varied. The results are shown in Figure 6 and tabulated in Table 2. Note from Table 2 that the phase ripple has a minimum whereas the amplitude ripple stays constant.

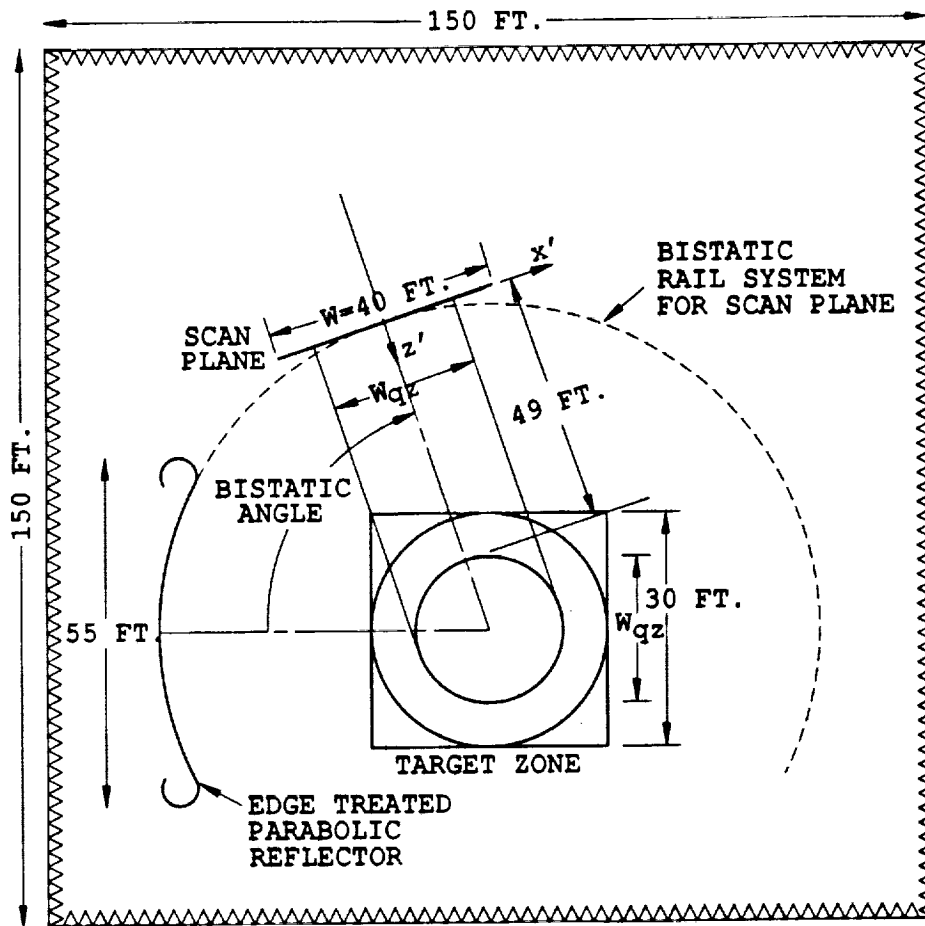


Figure 5: Bistatic RCS Measurement Facility with Planar Scanner

1GHz D=12.49m Taper 12 14 16%,90° $\Delta S=0.5\lambda$

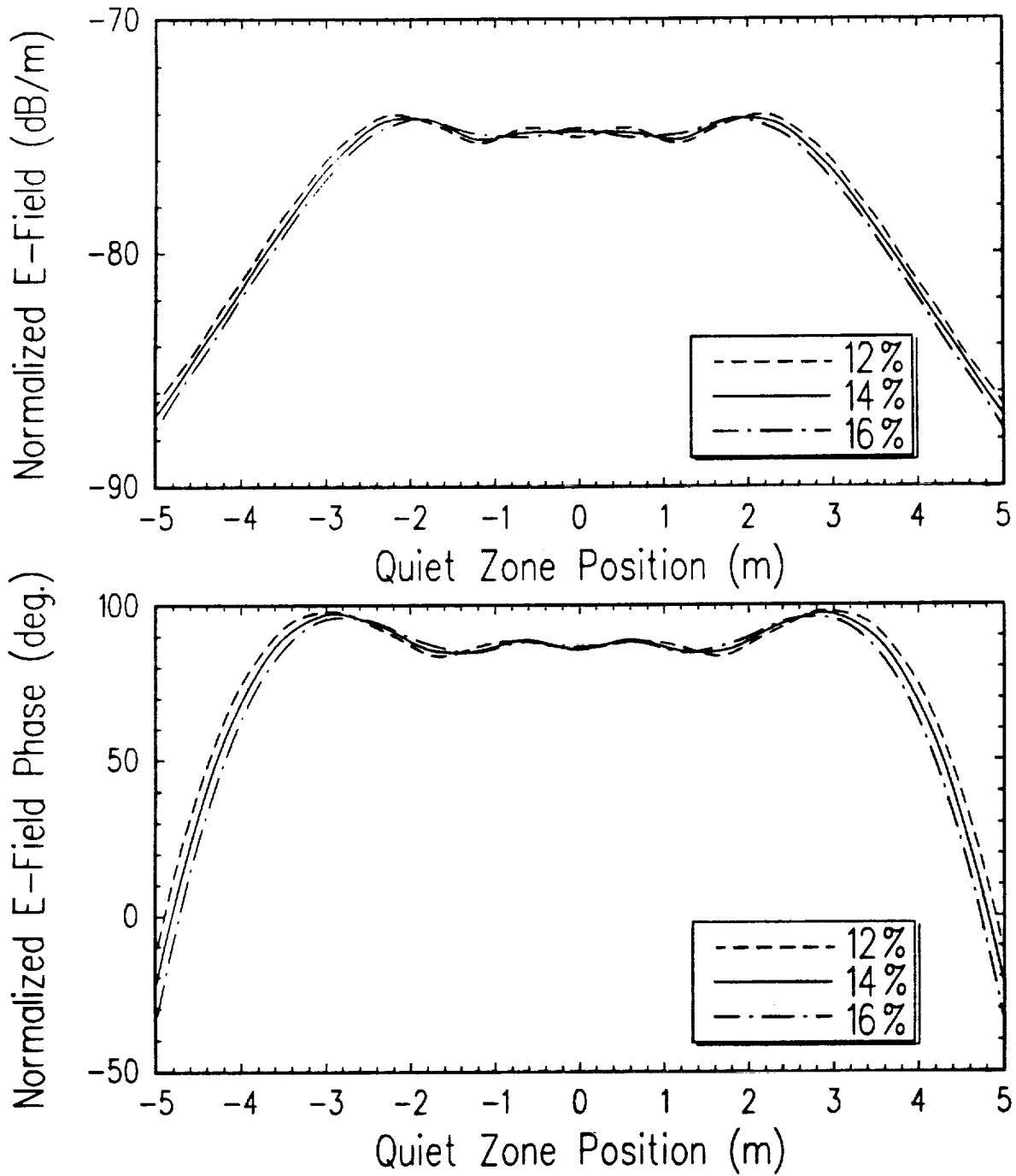


Figure 6: Normalized E-Field Amplitude and Phase, Comparison of Different Amounts of Amplitude Taper

Table 2: Scan Plane Array Antenna Amplitude Taper Response, 90°

Taper [%]	Ripple [dB]	Ripple [deg]	$W_{gz}$ [m]	Size Ratio
12	1.2	15	5.6	1.52
13	1.1	13	5.4	1.57
14	1.0	11	5.2	1.63
16	1.0	12	5.2	1.63

Table 3: Scan Plane Array Antenna Phase Taper Response, 12%

Taper [deg]	Ripple [dB]	Ripple [deg]	$W_{gz}$ [m]	Size Ratio
45	1.5	12	5.0	1.70
90	1.2	15	5.6	1.52
135	1.1	13	5.4	1.57
180	1.0	12	5.4	1.57

Next the amplitude taper was held constant at 12%, and the phase taper was varied to try to bring the ripple to within the 1 dB, 10° specifications. The results of this are shown in Figure 7 and tabulated in Table 3. From Tables 2 and 3, note that similar responses were obtained for tapers of 12%,180° and 14%, 90°. We chose the 14%, 90° taper for the tests to follow, leaving more room for variation of the phase taper if necessary.

### 3.4.2 Sample Spacing

Figures 8, 9 and 10 illustrate the effect of element spacing greater than  $\lambda/2$  at 1, 10 and 18 GHz respectively. The amplitude and phase ripple are summarized in Table 4. It is apparent from these figures that a sample

1GHz D=12.49m Taper 12%, 45° 90° 180°  $\Delta S = 0.5\lambda$

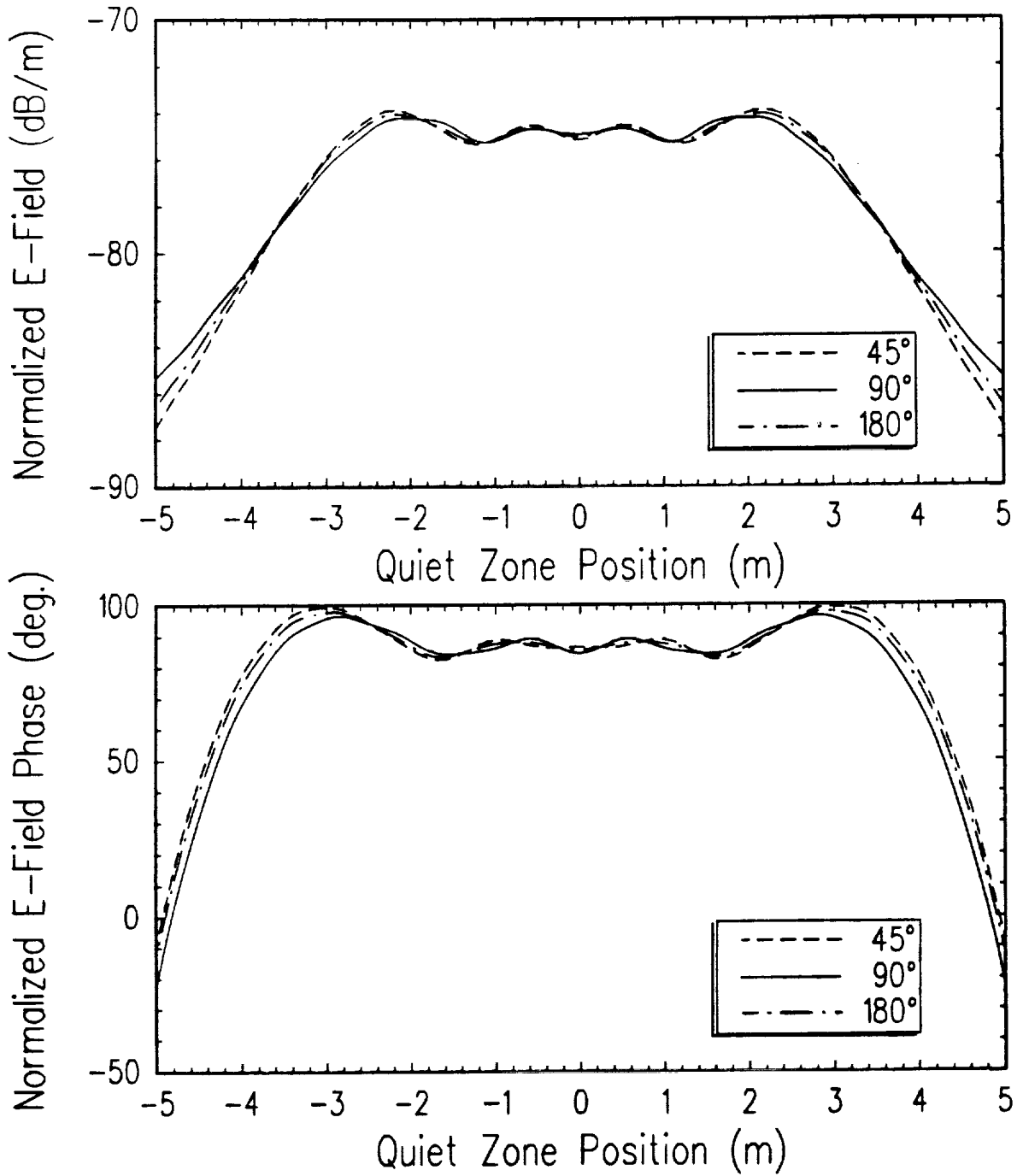


Figure 7: Normalized E-Field Amplitude and Phase, Comparison of Different Amounts of Phase Taper

Table 4: Scan Plane Array Antenna Sample Spacing Variation Response

f [GHz]	Spacing [ $\lambda$ ]	Ripple [dB]	Ripple [deg]	$W_{qz}$ [m]	Size Ratio
1.0	0.5	1	11	5.2	1.63
	1.0	1	12	5.6	1.52
	1.5	2	20	5.6	1.52
	2.0	5	24	4.0	2.13
	2.5	8	67	2.2	3.86
10.0	0.5	1	3	6.4	1.33
	1.0	1	3	6.4	1.33
	1.5	1	3	6.4	1.33
	1.75	1	3	6.4	1.33
	2.0	1	9	5.8	1.47
	2.5	1	12	2.6	3.27
18.0	0.5	1	3	6.6	1.29
	1.0	1	3	6.6	1.29
	1.5	1	3	6.6	1.29
	1.75	1	3	6.6	1.29
	2.0	1	9	6.2	1.37
	2.5	1	12	2.8	3.04

spacing of  $1.75\lambda$  is satisfactory for the higher frequencies, but at 1 GHz,  $1\lambda$  is the largest satisfactory spacing. It can be calculated from Table 4 that an element spacing of 2.6 cm in the scan plane is acceptable for all frequencies below 18 GHz. The reason that  $2\lambda$  spacing has a poor quiet zone width is the close proximity of the grating lobes to the main beam of the antenna array in the scan plane.

1GHz D=12.49m Taper 14%,90°  $\Delta S=0.5$  1.0 1.5 $\lambda$

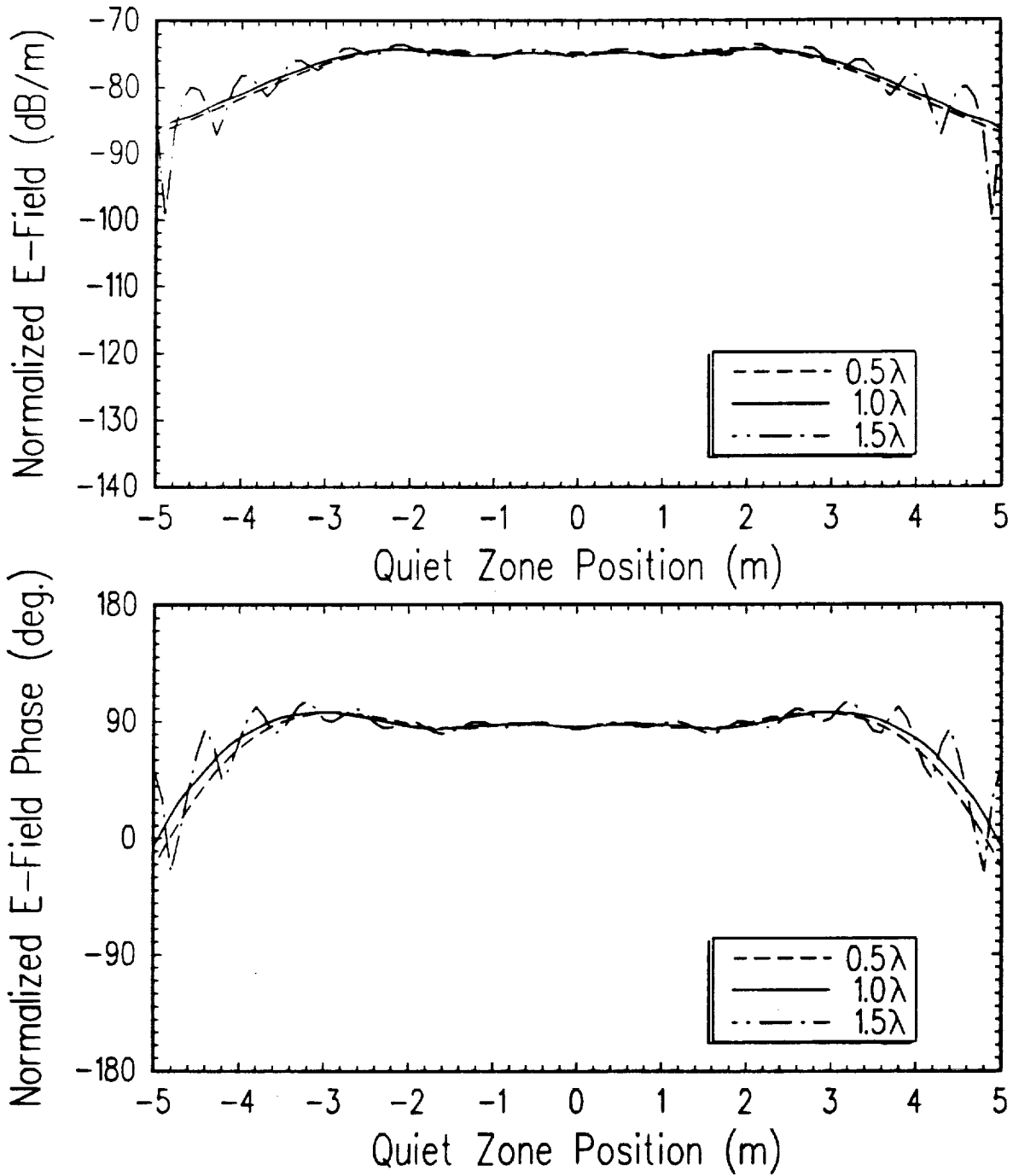


Figure 8: Normalized E-Field Amplitude and Phase, Comparison of Different Sample Spacings at 1 GHz

10GHz D=12.49m Taper 14%,90°  $\Delta S=0.5$  1.75  $2\lambda$

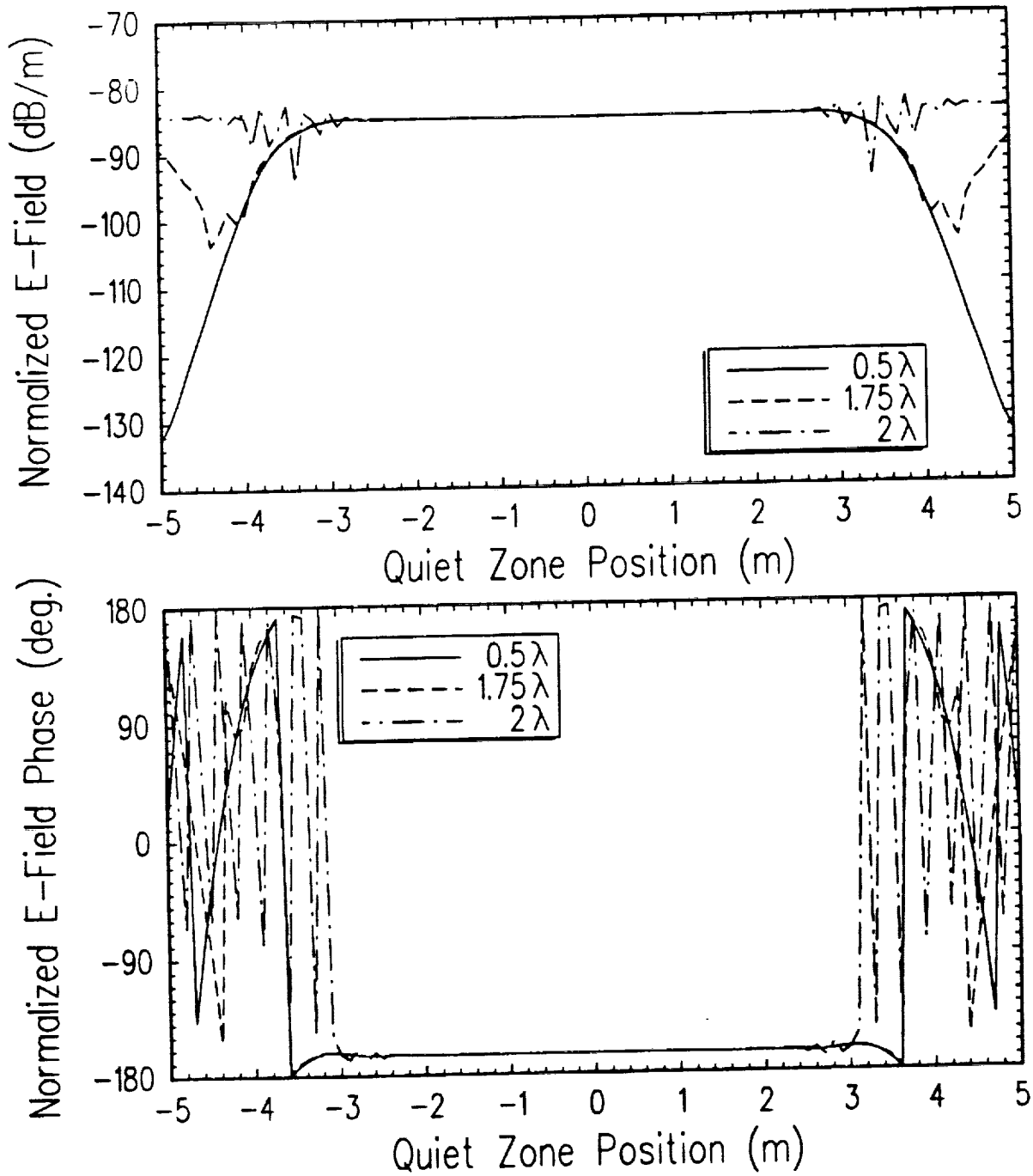


Figure 9: Normalized E-Field Amplitude and Phase, Comparison of Different Sample Spacings at 10 GHz

18GHz D=12.49m Taper 14%,90°  $\Delta S=0.5$  1.75  $2\lambda$

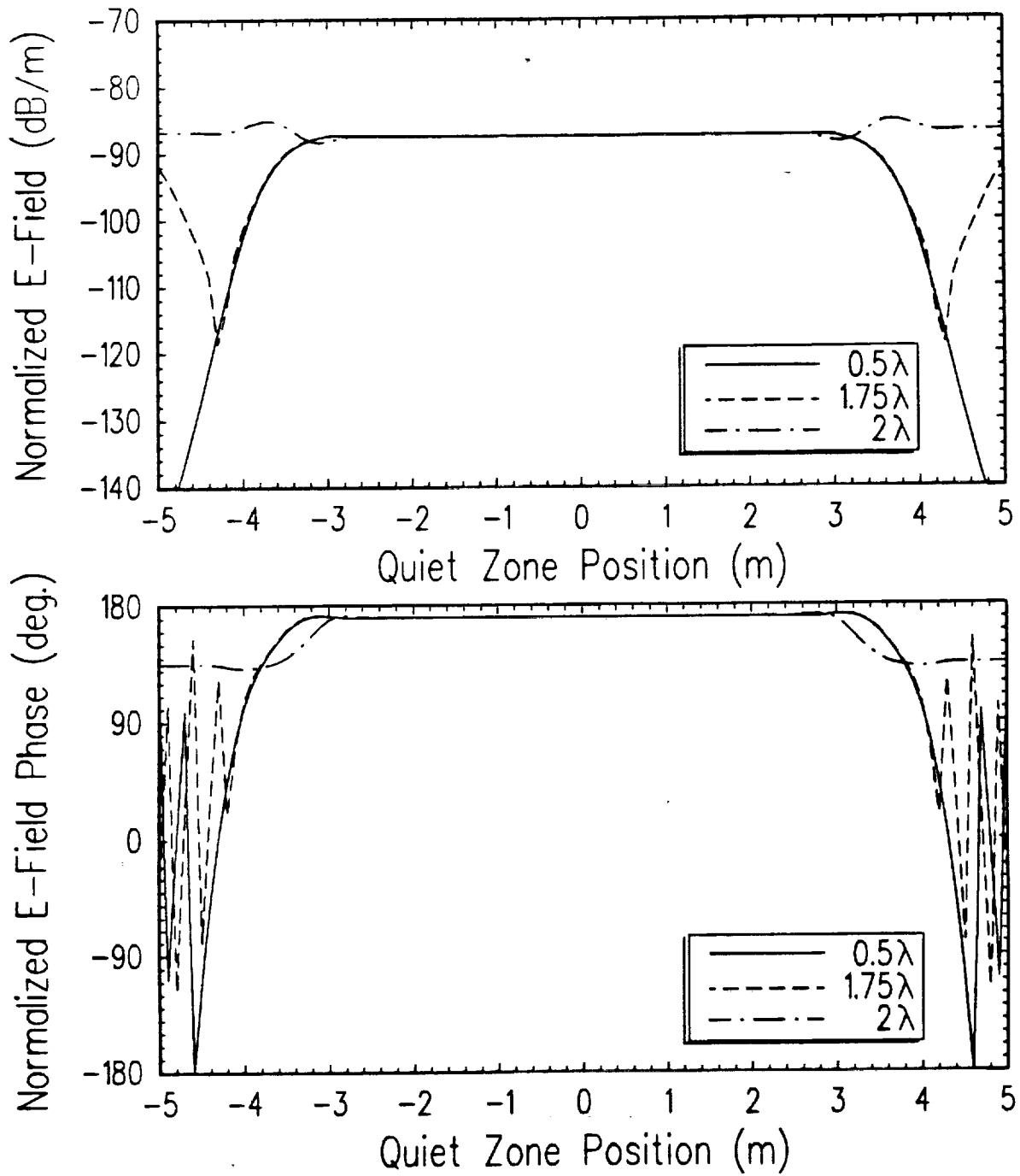


Figure 10: Normalized E-Field Amplitude and Phase, Comparison of Different Sample Spacings at 18 GHz

### 3.4.3 Aperture Size

For a worst case of  $1.0\lambda$  spacing at 1 GHz, our design gives a scan-plane to target-zone size ratio of 1.5, see Table 4. This is an improvement over the scanners mentioned in the literature which have size ratios only as low as 1.7, and it is much smaller than the OSU compact range reflector ratio. For the OSU compact range reflector at 1 GHz, the amplitude ripple is 1 dB and the phase ripple is  $10^\circ$  over a 2.7 m quiet zone height [11 p179 Fig.10(a)]. Dividing the nominal height of the compact range reflector (5.8 m) by the quiet zone height results in a scan-plane to target-zone ratio of 2.1 .

### 3.4.4 Down Range Variation

Figures 11 and 12 illustrate the performance over the front, middle and back of the quiet zone for frequencies of 1 and 18 GHz respectively. At 1 GHz, even though the responses are all within a 1 dB ripple, the distance change causes differing ripple functions as the range increases. This indicates a  $z'$  dependence of the plane wave approximation which must be minimized. For 18 GHz, the ripple functions are all well suppressed and no  $z'$  dependence is observed. The results of these test are given in Table 5.

### 3.4.5 Outside Design Frequency Band

The last two figures, 13 and 14, show the response of the scanner array to the frequencies 0.5 and 35 GHz which are outside the design frequency band of 1 to 18 GHz. The ripple is tabulated in Table 3. Note that a

1GHz D=10.37 12.49 14.61m Taper 14%,90°  $\Delta S=0.5\lambda$

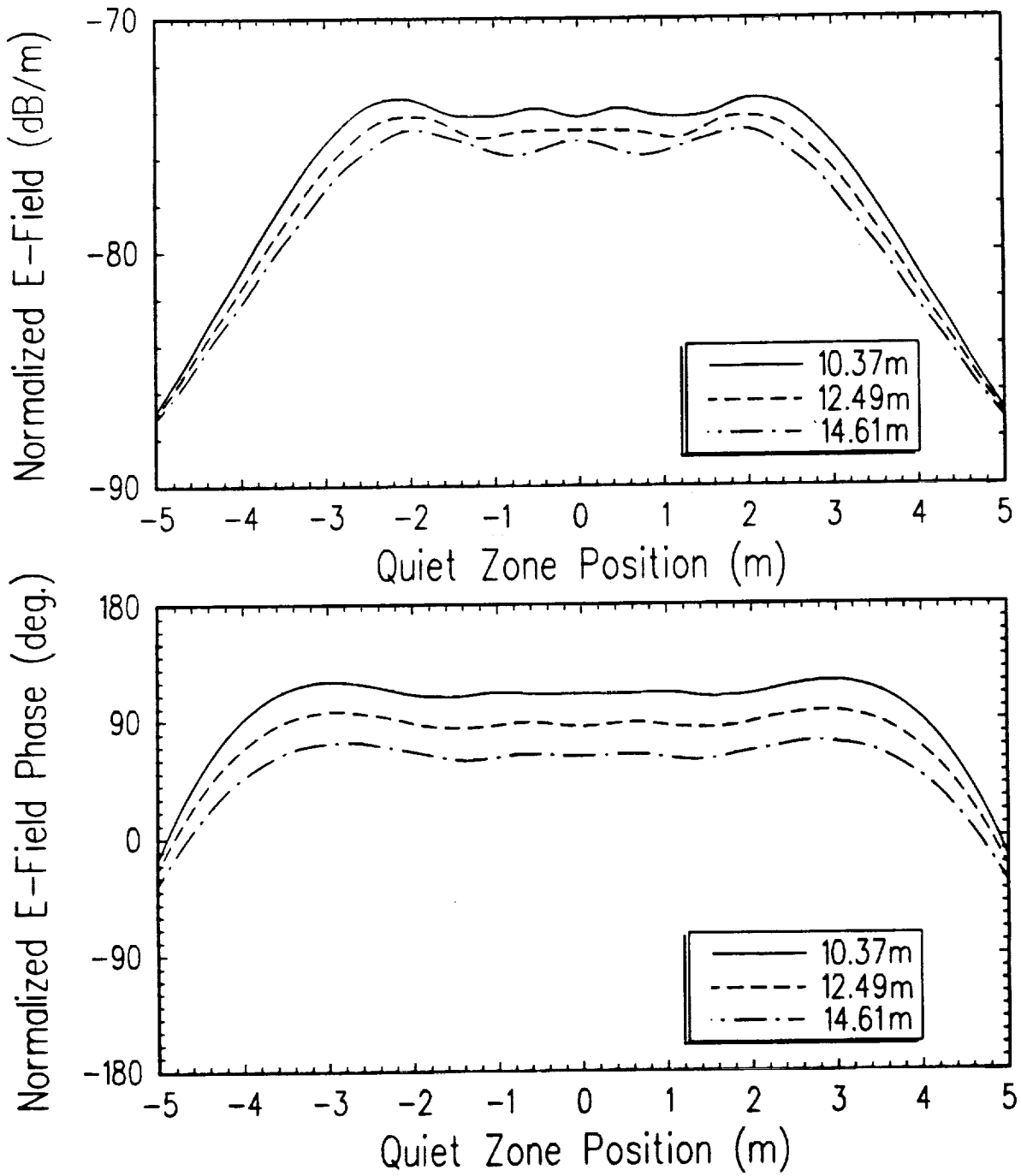


Figure 11: Normalized E-Field Amplitude and Phase, 1 GHz Down Range Response Comparison

18GHz D=10.37 12.49 14.61m Taper 14%,90°  $\Delta S=0.5\lambda$

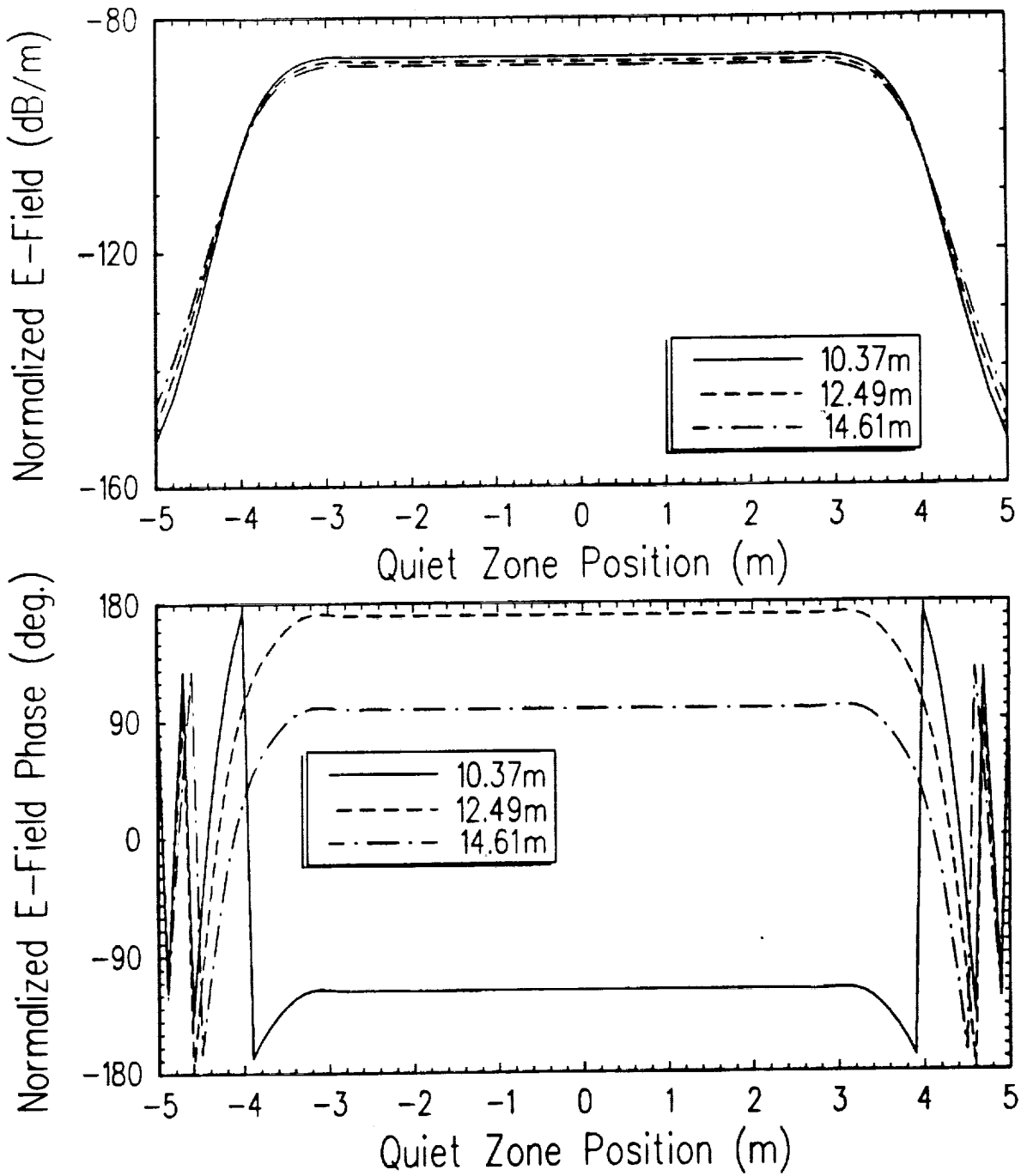


Figure 12: Normalized E-Field Amplitude and Phase, 18 GHz Down Range Response Comparison

Table 5: Scan Plane Array Antenna Down Range Performance

f [GHz]	Range [m]	Ripple [dB]	Ripple [deg]	$W_{gz}$ [m]	Size Ratio
1.0	10.37	1	10	6.0	1.42
	12.49	1	11	5.2	1.63
	14.61	1	14	5.4	1.57
18.0	10.37	1	3	6.6	1.29
	12.49	1	3	6.6	1.29
	14.61	1	3	6.6	1.29

Table 6: Scan Plane Array Antenna Performance Outside Design Band

f [GHz]	Spacing [ $\lambda$ ]	Taper [% ,deg.]	Ripple [dB,deg.]	$W_{gz}$ [m]	Size Ratio
0.5	0.5	14,90	1,12	3.8	2.24
35.0	0.5	22,135	1,3	6.6	1.29

minimum scan-plane to target-zone ratio of 2.2 at 0.5 GHz still compares well with the OSU compact range ratio of 2.1 at 1 GHz.

0.5GHz D=12.49m Toper 22%,135° $\Delta S=0.5\lambda$

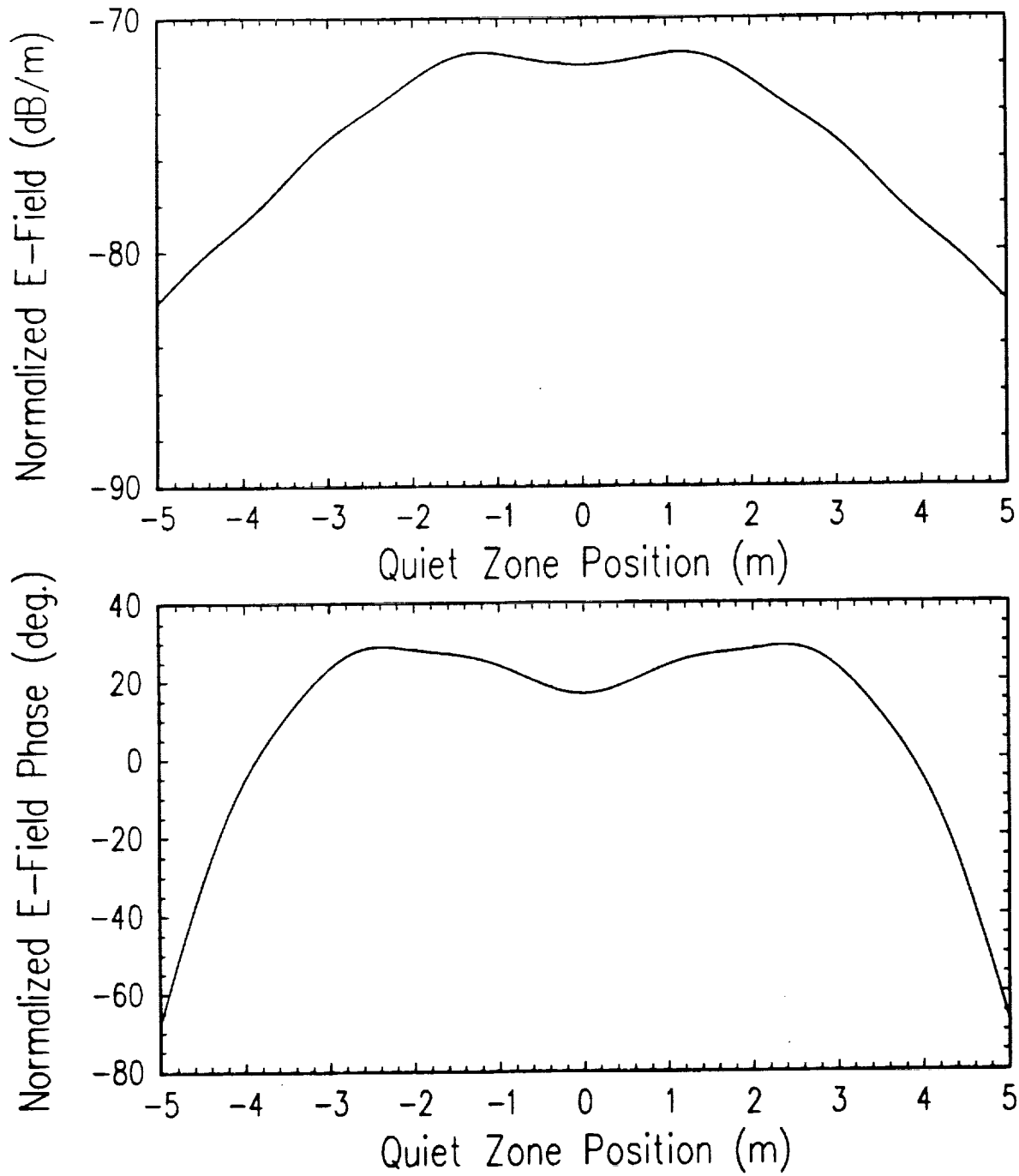


Figure 13: Normalized E-Field Amplitude and Phase, 0.5 GHz Response: Below Design Frequency Band

35GHz D=12.49m Taper 14%,90°  $\Delta S=1.75\lambda$

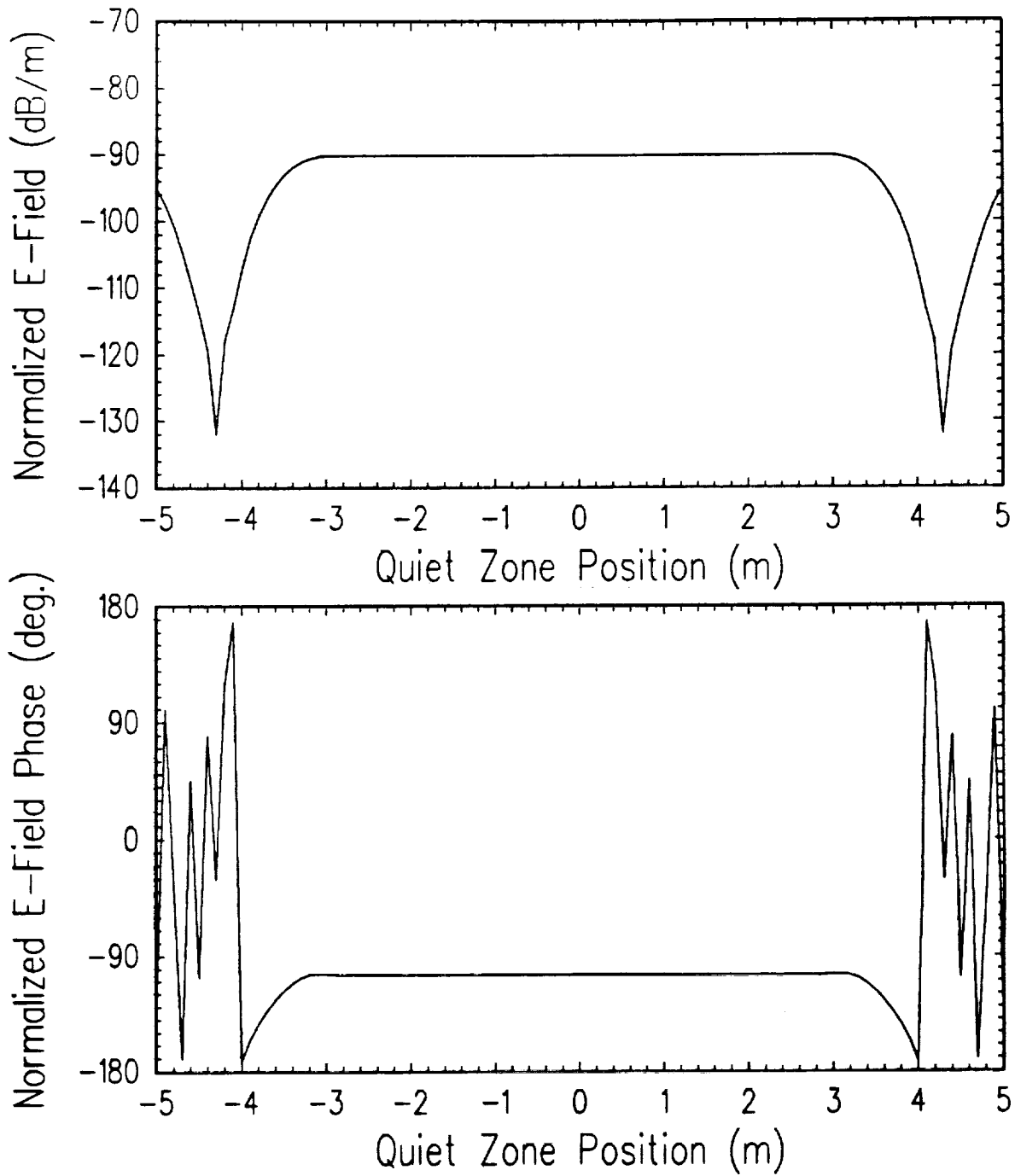


Figure 14: Normalized E-Field Amplitude and Phase, 35 GHz Response: Above Design Frequency Band

# Chapter 4

## Conclusions

The one dimensional results given above are directly applicable to the two dimensional case with possibly slight modifications to the windowing functions. The sample spacing tests suggest the use of a constant separation of the elements in the array (or the probe sample spacing), making the sample spacing independent of the frequency. The maximum theoretical spacing of  $2.8\lambda$  however, is not attainable due to the close proximity of the grating lobes. The variable distance tests indicate a need to quantify the  $z'$  dependence effect and reduce it for low frequencies. The tests outside the design band indicate a possibility to use these frequencies with some modification to the filtering or tapering functions and a possible decrease in target-zone width. An advantage of this planar scanning system is that performance modifications can be accomplished without hardware adjustment. Modifications or upgrades are done only on the processing algorithms.

# Chapter 5

## Future Work

### 5.1 Scanner Construction

To complete this project, we will build a prototype scanner to test the theoretical computations presented and to expand to the two dimensional case. We will test the necessity of optical/laser position tracking systems using computer error modeling as well as direct manipulation of the scanner. We will try to quantify the  $z'$  dependence of the fields at low frequencies and will try to find or develop an optimal filtering function of the scan plane antenna elements. We will extend the scope of the scanning process to theoretically evaluate the behavior of a scanner based on a scanning parabolic strip.

### 5.2 RCS Calibration Technique

Once the scanner has been designed and is operational, it can be used to measure calibrated bistatic RCS. The process of measuring bistatic RCS is similar to that for monostatic RCS. In contrast to a compact range reflector

system, planar scanner data sets need spatial filtering before being used to find the bistatic RCS. The measurement steps are as follows: (1) Scan a calibration target, usually a sphere. (2) Scan the background. (3) Vector subtract the background from the calibration target data set. (4) Apply theoretical bistatic RCS of sphere to normalize the experimental value obtained.

# Bibliography

- [1] R.C. Johnson, H.A. Ecker and J.S. Hollis "Determination of Far-Field Antenna Patterns from Near-Field Measurements" Proc. IEEE, vol. 61, No. 12, Dec. 1973 pp.1668-1694
- [2] A.D. Yaghjian "An Overview Of Near-Field Antenna Measurements" Trans. AP-S, vol. AP-34, No. 1, Jan. 1986 pp.30-45
- [3] E.B. Joy and D.T. Paris "Spatial Sampling and Filtering in Near-Field Measurements" Trans. AP-S, vol. AP-20 No. 3, May 1972 pp.253-261
- [4] E.B. Joy "Near-Field Range Qualification Methodology" Trans. AP-S, vol. AP-36, No. 6, June 1988 pp. 836-843
- [5] J.H. Bearden and A.D. Dugenske "A Planar Near-Field Positioner" Proc. AMTA 1988 pp. 13-9-13-12
- [6] H.G. Booker and P.C. Clemmow "The Concept of an Angular Spectrum of Plane Waves, and its relation to that of Polar Diagram and Aperture Distribution" Proc. IEE, vol. 97 pt.3 pp.11-17
- [7] D.T. Paris, W.M. Leach, Jr. and E.B. Joy "Basic Theory of Probe-Compensated Near-Field Measurements" Trans. AP-S, vol. AP-26, No. 3, May 1978 pp.373-379
- [8] A.D Yaghjian "Upper-Bound Errors in Far-Field Antenna Parameters Determined from Near-Field Measurements. Part 1: Analysis" NBS Tech. Note 667, Oct. 1975
- [9] B.J. Cown and C.E. Ryan, Jr. "Near-Field Scattering Measurements for Determining Complex Target RCS" Trans. AP-S, vol.37, No.5, May 1989 pp.576-585

- [10] D.M. Kerns "Plane-Wave Scattering Matrix Theory of Antennas and Antenna-Antenna Interactions." NBS Monograph 162, June 1981
- [11] W.D. Burnside, M.C. Gilreath, B.M. Kent and G.L. Clerici "Curved Edge Modifications of Compact Range Reflector" Trans. AP-S, vol. AP-35, No. 2, Feb. 1987 pp. 176-182

# **Appendix A**

## **C Program Listing**

```

#include <stdio.h>
#include <math.h>
#define MAX_IO_PTS 2000
#define MAX_IO_COL 4
#include <USER1:[REUNING.C.INCLUDE]DEF.H>

/* This program computes the fields in the quiet zone from an aperture */

/*****
/* Write data to FileName, w/header
*****/
void WriteFile(DataBlk,numpts,numcol,title,axisitles,FileName)
double DataBlk[MAX_IO_COL][MAX_IO_PTS];          /* data to print */
int numpts,                                     /* array access */
numcol;                                         /* number of columns */
char *title,                                    /* data graph titles */
*axisitles,                                    /* axis title array */
*FileName;                                     /* output file name */
{
int LCV,LCV2;                                  /* loop control variables */
FILE *outfileptr;                             /* output file pointer */

if ( (outfileptr = fopen(FileName, "w")) != NULL) /* file open error? */
{
printf("\nWriting %d columns to %s .\n\n",numcol,FileName); /* info */
printf("%s",title); /* print the titles */
fprintf(outfileptr,"%s",title);
printf("%s",axisitles); /* print the axis titles */
fprintf(outfileptr,"%s",axisitles);

for (LCV = 0; LCV <= numpts-1; LCV++) /* print the data */
{
for (LCV2 = 0; LCV2 <= numcol-1; LCV2++)
fprintf(outfileptr,"%lf ",DataBlk[LCV2][LCV]);
fprintf(outfileptr,"\n");
}
fclose(outfileptr); /* close output file */
printf("Write Completed\n"); /* user info output */
}
else /* error handler */
printf("Could not open filename = %s .\n",FileName);
} /* end procedure WriteFile */

/*****
/* Main
*****/
main()
{
/*****
/* declare variables */
*****/

char outfilename[60], /* filename variable */
title[120], /* data graph titles */
maintitle[50], /* main title string */
subtitle[70], /* subtitle string */
axisitles[120], /* axis title array */
xaxistitle[35], /* x title both graphs */
yaxistitle[35], /* y1 axis title */
y2axistitle[35]; /* y2 axis title */

double freq, /* operating frequency in GHz */
lambda, /* wavelength in cm */

```

```

        dist,          /* separation of aperture and quiet zone in cm */
        apln,         /* aperture length in cm */
        exhalfapln,  /* half+ the aperture length in cm */
        apsp,        /* aperture spacing in cm */
        qzln,        /* quiet zone length in cm */
        qzsp,        /* quiet zone spacing in cm */
        rolloff,     /* roll-off in amplitude/phase taper in cm */
        maxphsdlay;  /* max phase taper delay in degrees */

int      numap,      /* number points in aperture */
        numqz,      /* number points in quiet zone */
        testid,     /* test id number */
        lcv, lcv2;  /* loop control variables */

double   apem[MAX_IO_PTS], /* aperture E field magnitude in V/m */
        apep[MAX_IO_PTS], /* aperture E field phase in radians */
        apex[MAX_IO_PTS], /* aperture E field X coordinate in cm */
        apey[MAX_IO_PTS]; /* aperture E field Y coordinate in cm */

double   qzem[MAX_IO_PTS], /* quiet zone E field magnitude in V/m */
        qzep[MAX_IO_PTS], /* quiet zone E field phase in radians */
        qzex[MAX_IO_PTS], /* quiet zone E field X coordinate in cm */
        qzey[MAX_IO_PTS]; /* quiet zone E field Y coordinate in cm */

double   block[MAX_IO_COL][MAX_IO_PTS]; /* data block for file I/O */

double   R,          /* length between current point antennas in cm */
        Theta,      /* angle of exit from aperture in radians */
        PAT;        /* element pattern: function of Theta */

complex  Eap[MAX_IO_PTS], /* aperture E field */
        Eqz[MAX_IO_PTS], /* quiet zone E field */
        Etemp, CurEle; /* temporary variables to use in summation */

/*****
/* function declarations
*****/
complex C_add(),C_sub(), /* complex addition and subtraction */
        C_rect(),C_init(), /* convert to rect format and initialization */
        C_mult(),C_exp(); /* complex multiplication and exp function */

double  get_double(), /* function to get user input */
        pow(), /* exponentiation function */
        atan2(), /* arctangent function */
        cos(), /* cosine function */
        log10(), /* log base 10 function */
        C_mag(), /* returns the magnitude of a complex number */
        C_ang(); /* returns the arguement of a complex number */

int      get_int(); /* user input function */

/*****
/* input the general setup of the test
*****/

testid = get_int("\nEnter the test ID number ==>",0,0);
freq = get_double("\nEnter the FREQUENCY in GHz ==>",0.5,40.0);

lambda = 30.0/freq; /* in cm */

dist = get_double("\nEnter the SEPARATION in m ==>",0.0,40.0)*100.0;
apsp = get_double("\nAperture ELEMENT SPACING in WAVELENGTHS ==>",
        0.0,5.0)*lambda;
apl = get_double("\nMaximum Aperture WIDTH in m ==>",0.0,20.0)*100.0;

numap = (apl/apsp)+1;

```

```

apln = (numap-1)*apsp; /* the exact length */
exhalfapln = aplan/2.0 + apsp;
if(numap >= MAX_IO_PTS-1) printf("\nNumber of elements exceeds array size.");

qzln = get_double("\nMaximum Quiet Zone WIDTH in m ==>",0.0,20.0)*100.0;
qzsp = qzln/100.0; /* in cm. ensures 100 points in the quiet zone */

numqz = (qzln/qzsp)+1;
qzln = (numqz-1)*qzsp; /* the exact length */
if(numqz >= MAX_IO_PTS-1) printf("\nNumber of elements exceeds array size.");

rolloff = (get_double("\nROLLOFF percentage ==>",0.0,50.0)/100.0)*apln;
maxphsdlay = get_double("\nMax. PHASE LAG in degrees ==>",0.0,360.0);
printf("Enter a main title.\n");
gets(maintitle); /* discard the return from the previous input */
gets(maintitle);

/*****
/* set up the position of aperture and quiet zone arrays */
*****/
for(lcv=0;lcv<=numap-1;lcv++)
{
    apex[lcv]=0.0;
    apey[lcv]=(apln/2.0)-((lcv)*apsp);
}

for(lcv2=0;lcv2<=numqz-1;lcv2++)
{
    qzex[lcv2]=dist;
    qzey[lcv2]=(qzln/2.0)-((lcv2)*qzsp);
}

/*****
/* set up the values of the aperture arrays */
*****/
for(lcv=0;lcv<=numap-1;lcv++)
{
    /* Amplitude taper in V/m. can be any function of position (lcv) */
    if (apey[lcv] <= exhalfapln &&
        apey[lcv] >= exhalfapln - rolloff &&
        rolloff != 0.0)
    {
        apem[lcv]= (pow(cos((PI/(2*rolloff)))*(apey[lcv]-exhalfapln+rolloff)),
            2.0)/numap;
    }
    else if(apey[lcv] >= -exhalfapln &&
        apey[lcv] <= -exhalfapln + rolloff &&
        rolloff != 0.0)
    {
        apem[lcv]= (pow(cos((PI/(2*rolloff)))*(apey[lcv]+exhalfapln) +
            (PI/2.0)),2.0)/numap;
    }
    else
    {
        apem[lcv]= (1.0/numap);
    }

    /* Phase taper in radians can be any function of position */
    if(apey[lcv] <= exhalfapln && apey[lcv] >= exhalfapln - rolloff)
    {
        apeg[lcv]= maxphsdlay*(PI/180.0)*(sin((PI/(2.0*rolloff))*
            (apey[lcv]-exhalfapln+rolloff)+PI/2.0)-1);
    }
    else if(apey[lcv] >= -exhalfapln && apey[lcv] <= -exhalfapln + rolloff)
    {
        apeg[lcv]= maxphsdlay*(PI/180.0)*(sin((PI/(2.0*rolloff))*
            (apey[lcv]+exhalfapln))-1);
    }
}

```

```

    }
    else
    {
        apep[lcv]= 0.0;
    }

    /* combine into a complex number */
    Eap[lcv]=C_rect(C_init(apem[lcv],apep[lcv]*180.0/3.14159265359));
}

printf("\nProcessing...\n"); /* user information */
/*****
/* calculate the quiet zone fields */
*****/
for(lcv2=0;lcv2<=numqz-1;lcv2++)
{
    Etemp=C_init(0.0,0.0);
    for(lcv=0;lcv<=numap-1;lcv++)
    {
        R = pow((pow(dist,2.0)+pow(apey[lcv]-qzey[lcv2],2.0)),0.5);
        Theta = atan2((apey[lcv]-qzey[lcv2]),pow(dist,2.0));
        PAT = 1; /* any function of Theta */

        CurEle = C_mult(C_mult(Eap[lcv] , C_init((PAT/R),0.0) ),
            C_exp( C_init(0.0,-2*3.14159265359/lambda*R) ) );

        Etemp = C_add(Etemp,CurEle);
    }
    Eqz[lcv2] = Etemp;
    qzem[lcv2] = 20.0*log10(C_mag(Eqz[lcv2])); /* in dB/m */
    qzep[lcv2] = C_ang(Eqz[lcv2]); /* in degrees */
}

/*****
/* output y coordinate, magnitude & phase */
*****/

sprintf(outfilename,"QZ%03d.dat",testid); /* plot title generation */
sprintf(subtitle,
"%gGHz D=%gm Taper %g \", %g S=%g \",
freq,dist/100.0,rolloff/apln*100.0,maxphsdlay,apsp/lambda);
sprintf(title,"%s %d\n%s\n",maintitle,testid,subtitle);
sprintf(xaxistitle,"[1]Quiet Zone Position (m)");
sprintf(yaxistitle,"[2]Normalized E-Field (dB/m)");
sprintf(y2axistitle,"[3]Normalized E-Field Phase (deg.)");
sprintf(axistitles,"%s\n%s\n%s\n",xaxistitle,yaxistitle,y2axistitle);

printf("\nStoring...\n");

for(lcv=0;lcv<=numqz-1;lcv++) /* put data into the data block */
{
    block[0][lcv]=qzey[lcv]/100.0;
    block[1][lcv]=qzem[lcv];
    block[2][lcv]=qzep[lcv];
}
WriteFile(block,numqz,3,title,axistitles,outfilename);
}

```

